Hydrostatic extrusion of linear polyethylene

The work described is part of an investigation of the hydrostatic extrusion of polymeric materials and is restricted to the results of a preliminary study of the hydrostatic extrusion of linear polyethylene (BP "Rigidex 50") at a temperature below its melting point.

Much recent work on deformation of linear polyethylene (LPE) in various processes has been performed with the incentive of approaching, in a highly oriented bulk material, the theoretical stiffness of a fully aligned system of chains [1].

A number of workers, notably Porter *et al* [2] have studied the material produced when a polymer at a temperature just above its melting point is subject to elongation, shear and pressure in a capillary rheometer. The strands produced have a high axial stiffness, and are believed to consist of a core of chain-extended fibrils surrounded by a sheath of chain-folded material.

A number of other workers, operating in the solid phase, have succeeded in producing highly deformed material using a piston-cylinder apparatus with a convergent die. For example, with this approach Imada *et al.* [3] have achieved an extensional modulus of 30 GN m^{-2} in a highly transparent product, whilst Predecki and Statton [4], using pressures up to 20 kbar attained deformation ratios of up to 36, but quote a lower stiffness.

The process of hydrostatic extrusion, where the ram or piston is not in direct contact with the deforming material, has some advantages over the conventional piston-cylinder apparatus [5, 6]. Frictional forces between the billet and the container wall are eliminated as the billet is surrounded by fluid, and die friction is also reduced by the presence of a pressurised lubricant. For these reasons the pressures required for hydrostatic extrusion are lower, and the deformation which takes place approximates more closely to convergent flow.

In the present work, Rigidex 50 linear polyethylene ($\bar{M}_w$ = 67 800; $\bar{M}_n$ = 13 350) [7] has been hydrostatically extruded at 100°C. The highest deformation ratio attained so far is 25 and the stiffness of this material was 46 GN m^{-2}. The billets for hydrostatic extrusion were machined from compression-moulded rods which were prepared by melting granules of polymer at 170°C and subjecting them to a combination of pressure and cooling. The billets used had a density of 0.971 ± 0.002.

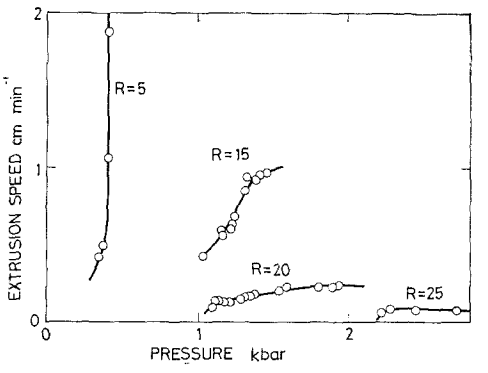

Figure 1 Variation of extrusion speed with pressure for Rigidex 50 LPE hydrostatically extruded to different deformation ratios at 100°C.

The extrusions were performed using 15° semi-angle dies with bores of 2.50 and 2.18 mm. The smaller die was used at deformation ratios above 20, as the internal diameter of the pressure vessel limited the size of billet which could be used. It was found advantageous to machine a generous radius at the transition between the deformation zone and the die bore. Castor oil was used as the pressure-transmitting fluid, and the billets were coated with silicone vacuum grease which acted as a lubricant. A small tensile stress was applied to the extrudate in order to maintain a straight product. At low deformation ratios the extrudate was opaque, and swelling occurred at the die exit. However, at intermediate deformation ratios (in the range 6 to 10) the extrudates became progressively clearer and ceased to swell upon leaving the die.

The change in appearance of the product was accompanied by a change in the characteristics of the extrusion process. Fig. 1 shows the relation between extrusion speed and extrusion pressure for different deformation ratios. At low deformation ratios the extrusion speed can be varied over a wide range without changing the pressure very much. At high deformation ratios, however, the speed is much lower, and changing the pressure has very little effect upon it.

At deformation ratios above 10, the product was hard, stiff, and highly transparent. The optical birefringence (Fig. 2) begins to approach a steady value in about the same region as the transition in extrusion behaviour.

Axial stiffness was measured using an Instron

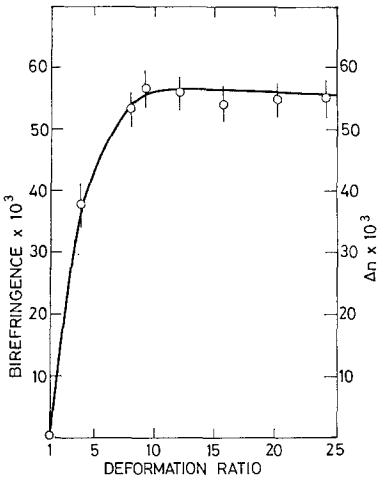

Figure 2 Variation of birefringence with deformation ratio.

testing machine equipped with a strain-gauge extensometer. All moduli are secant moduli measured at 0.1% strain at 21°C and at a strain-rate of approximately 10^{-5} sec^{-1}. The relationship between modulus and deformation ratio is shown in Fig. 3.

Modulus increases with deformation ratio, but there is apparently an increase in slope at a deformation ratio of 10 (i.e. in the transition range of extrusion behaviour). The maximum value of modulus observed so far has been 46 GN m^{-2}, more than 28 times that of the isotropic material, and within a factor of 5 of most estimates of the ultimate modulus [1].

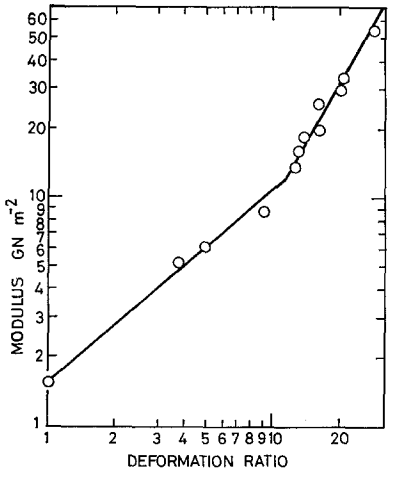

Figure 3 Effect of deformation ratio on the modulus of the extrudate.

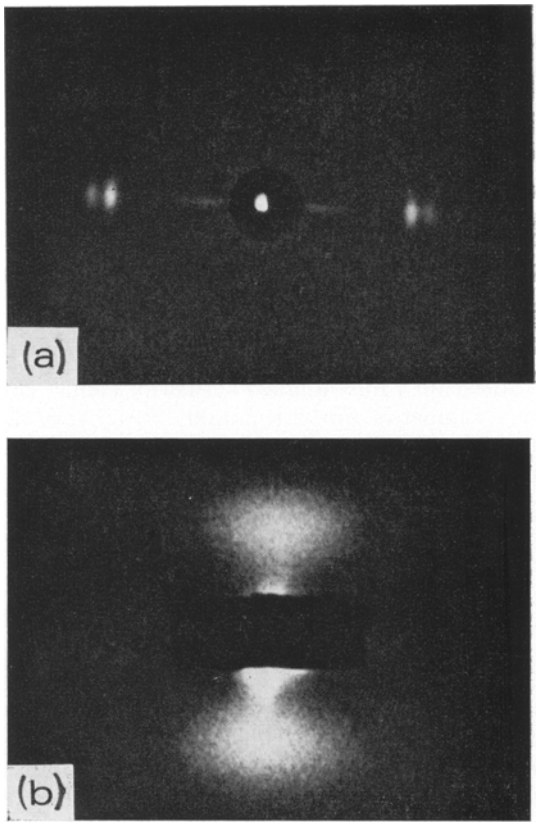

Figure 4 (a) Wide-angle X-ray picture and (b) low-angle X-ray picture of extrudate at a deformation ratio of 20.

Wide- and low-angle X-ray pictures of material at a deformation ratio of 20 show a high degree of orientation and a periodicity of about 200 Å. DTA results, corrected for heating rate, indicate a slight increase in melting point from 134° for the original material to 136° for the most highly deformed material. Clearly there is no extended chain material present.

It is generally understood that the axial stiffness of oriented crystalline polymers is greatly influenced by the nature of the coupling between crystalline regions [8]. In particular, "tie molecules" or "intercrystalline bridges" which transcend the disordered regions are believed to play an important part in determining stiffness.

Although it is not possible to quantify directly the amount of material constituting the tie molecules, an estimate can be made using a simplified model. A series crystalline-amorphous model is assumed, with a fraction of crystalline material transcending the amorphous zone.

The resulting expression (Equation 1) is identical with the model proposed by Takayanagi [9].

$$\frac{1}{E} = \frac{L-t}{L}\frac{1}{E_c} + \frac{t}{L}\frac{1}{XE_c + (1-X)E_A} \quad (1)$$

where E is the overall stiffness, L is the long period, t is the amorphous layer thickness, X is the fraction of crystalline tie material in the amorphous layer and E_c and E_A are the stiffnesses of crystalline and amorphous components respectively. These quantities are not all known accurately but within the terms of reference and limitations [8] of the model the following conclusions can be drawn:

1. The compliance of the amorphous layer which is the dominant factor in determining the overall compliance consists of two terms corresponding to the amorphous material and the tie material. When the overall stiffness is greater than about 10 GN m^{-2}, the contribution of the amorphous material is small compared with that of the tie-material.

2. It is possible to achieve a significant proportion of the ultimate stiffness with a relatively small proportion of tie material.

This could explain how it is possible to achieve a high modulus in a material which retains a periodicity of 200 Å.

The model also suggests a possible cause for the increase in slope of the modulus curve above a deformation ratio of 10, corresponding to a modulus of 10 GN m^{-2}. At deformation ratios below 10, factors such as crystalline orientation and the low stiffness of the amorphous material limit the stiffness and account for the slow increase with deformation ratio. At deformation ratios above 10 the tie material becomes dominant in determining the stiffness, and the more rapid rate of increase of stiffness must be due to the production of an increasing quantity of intercrystalline ties in the extrusion process.

The main drawback of the model is our ignorance of the nature of this intercrystalline material and of the constraints which apply to it. Nitric acid etching and broad-line NMR experiments are being undertaken in an attempt to learn more about this.

The deformation mechanisms in hydrostatic extrusion of LPE are not well understood, but it seems feasible that the process is qualitatively similar to that described by Peterlin [10] for drawing. Peterlin describes three stages in the drawing process: plastic deformation of the original spherulitic structure, discontinuous localised transformation from the spherulitic to fibre structure and finally plastic deformation of the fibre structure itself.

In hydrostatic extrusion the transition from spherulitic to fibre structure is a more gradual one as there is no macroscopic neck present, the flow pattern being determined by the geometry of the die. It does seem possible that the transformation still takes place by localized necking on a microscopic scale.

From the birefringence measurements it appears that the transformation to the fibre structure is essentially complete when a draw ratio of 10 has been reached. Further deformation beyond this point can only take place by deformation of the fibre structure itself.

The most likely deformation process at high deformation ratios is slip parallel to the *c*-axes and it seems possible that tie material plays an important part in this process. Deformation could be initiated locally at regions of high shear stress where tie material is connected to crystalline zones. This type of flow process involving *c*-axis slip could well be strongly affected by the normal stress acting on planes containing the *c*-axis (i.e. a localized Coulomb yield criterion could apply [11]). This would result in a pressure dependence of the flow stress and could account for the low deformation rates observed at high deformation ratios. A more detailed investigation into the process and properties of the extrudates is now underway.

The details of the preparation of the materials of high stiffness are the subject of a patent application (A. G. Gibson and I. M. Ward, U.K. Patent Appl. 30823/73 filed 28.6.73).

Acknowledgements

The work reported here forms part of a joint project involving the Departments of Physics and Mechanical Engineering at Leeds University and is supported by a research grant from the Science Research Council. The authors are indebted to Mr H. O'Hare for moulding and machining the billets for hydrostatic extrusion and to Mr R. N. Britton for the X-ray diffraction photographs.

References

1. F. C. FRANK, *Proc. Roy. Soc. Lond. A.* **319** (1970) 127.
2. J. H. SOUTHERN and R. S. PORTER, *J. Appl. Polymer Sci.* **14** (1970) 2305.

3. K. IMADA, T. YAMAMOTO, K. SHIGEMATSU and M. TAKAYANAGI, *J. Mater. Sci.* **6** (1971) 537.
4. P. PREDECKI and W. O. STATTON, *J. Polymer Sci.* **B10** (1972) 87.
5. H. L. D. PUGH, Bullied Memorial Lectures Vol. III University of Nottingham (1965).
6. T. WILLIAMS, *J. Mater. Sci.* **8** (1973) 59.
7. G. CAPACCIO and I. M. WARD, *Nature, Physical Science* **243** (1973) 143.
8. E. W. FISCHER, H. GODDAR and W. PIESCZEK, *J. Polymer Sci.* **C31** (1970) 87.
9. M. TAKAYANAGI, K. IMADA and T. KAJIYAMA, *ibid* **C15** (1966) 263.
10. A. PETERLIN, *J. Mater. Sci.* **6** (1971) 490.
11. A. KELLER and J. G. RIDER, *ibid* **1** (1966) 389.

Received 22 January
and accepted 29 January 1974

A. G. GIBSON
I. M. WARD
Department of Physics

B. N. COLE
B. PARSONS
Department of Mechanical Engineering,
University of Leeds,
Leeds, UK

Thermal expansion of zinc carbonate

In the course of X-ray investigations on calcite-type compounds, the authors have determined the precision lattice parameters and the coefficients of thermal expansion of a number of carbonates [1-3], nitrates [4, 5] and borates [6]. A perusal of the literature shows that the thermal expansion of zinc carbonate, which has the same structure as calcite, has not so far been studied. Hence, it is thought worthwhile to also include zinc carbonate as a part of a programme of X-ray studies on calcite-type compounds.

Transparent single crystals of zinc carbonate of rhombohedral shape were crushed to powder and the specimen for the study was prepared by coating the powder on to a quartz fibre with Quickfix. Using the Unicam high temperature camera, powder photographs were taken at different temperatures, in the temperature range 30 to 265° C with Cu*K* radiation from a Raymax-60 demountable X-ray unit. Five reflections, $(3.0.12)_{\alpha_1}$, $(416)_{\alpha_1}$, $(416)_{\alpha_2}$, $(2.1.16)_{\alpha_1}$ and $(2.1.16)_{\alpha_2}$ recorded between 56 and 73° Bragg angles were used in evaluating the lattice parameters at different temperatures. The experimental details and the method of evaluating the precision lattice parameters and the coefficients of thermal expansion were described in an earlier paper [1].

The lattice parameters determined at different temperatures are given in Table I. The lattice parameters at room temperature obtained in the present investigation are compared with the earlier values in Table II.

The temperature dependence of the coefficients of thermal expansion is represented by the following equations.

$$\alpha_{\parallel} = 23.001 \times 10^{-6} + 2.002 \times 10^{-8}T + 1.591 \times 10^{-11}T^2 \quad (1)$$

$$\alpha_{\perp} = 8.976 \times 10^{-6} + 3.179 \times 10^{-9}T + 2.567 \times 10^{-11}T^2 \quad (2)$$

TABLE I Lattice parameters of $ZnCO_3$ at different temperatures

Temperature (°C)	*a* (Å)	*c* (Å)
30	4.6646 ± 0.0004	15.1232 ± 0.0013
78	4.6659 ± 0.0004	15.1363 ± 0.0013
128	4.6692 ± 0.0004	15.1608 ± 0.0013
165	4.6722 ± 0.0004	15.1844 ± 0.0013
215	4.6737 ± 0.0004	15.1978 ± 0.0013
232	4.6740 ± 0.0004	15.2005 ± 0.0013
265	4.6753 ± 0.0004	15.2137 ± 0.0013

TABLE II Lattice parameters of $ZnCO_3$ at room temperature

Author	*a* (Å)	*c* (Å)
Swanson *et al.* [7]	4.6533	15.028
Graf [8]	4.6534	15.027
Present study	4.6646	15.1232

TABLE III Coefficients of thermal expansion of $ZnCO_3$ at different temperatures.

Temperature (°C)	$\alpha_{\parallel} \times 10^6$		$\alpha_{\perp} \times 10^6$	
	Obs.	Calc.	Obs.	Calc.
40	23.47	23.83	9.11	9.14
60	24.14	24.25	9.33	9.26
80	25.13	24.70	9.43	9.39
100	25.79	25.16	9.54	9.55
120	25.79	25.63	9.65	9.73
140	25.79	26.61	9.86	9.92
160	26.12	26.61	9.97	10.14
180	26.78	27.11	10.72	10.38
200	27.77	27.64	10.72	10.64
220	28.43	28.17	10.72	10.92
240	28.76	28.72	11.25	11.22